Asociación Argentina
de Mecánica Computacional

Mecánica Computacional Vol XXIX, págs. 5055-5068 (artículo completo)
Eduardo Dvorkin, Marcela Goldschmit, Mario Storti (Eds.)
Buenos Aires, Argentina, 15-18 Noviembre 2010

NUMERICAL PREDICTION OF THE SHOCK-WAVE STRUCTURE OVER A REENTRY BRAZILIAN CAPSULE

Wilson F. N. Santos

Combustion and Propulsion Laboratory (LCP), National Institute for Space Research (INPE), Cachoeira Paulista, SP, 12630-000, BRAZIL, wilson@lcp.inpe.br, http://www.lcp.inpe.br

Keywords: Hypersonic Flow, Rarefied Flow, DSMC, Reentry Capsule, Shock Wave.

Abstract. This work presents computational results of the shock-wave structure for typical hypersonic flow conditions encountered by the small ballistic reentry Brazilian vehicle SARA (acronyms for SAtélite de Reentrada Atmosférica). Most of the transition flow regime is covered by the altitude range of 120 to 80 km. Calculations were made with the Direct Simulation Monte Carlo (DSMC) method that accounts for translational, rotational, and vibrational non-equilibrium effects. The primary aim of this paper is to examine the behavior of the shock-wave structure during the high altitude portion of SARA reentry. In this fashion, the influence of rarefaction on the shock-wave standoff distance, shock-wave thickness, and shock-wave shape will be investigated for altitudes of 100, 95, 90, 85 and 80 km, and by a model that identifies the molecules in three distinct classes: (1) undisturbed freestream, (2) reflected from the body surface, and (3) scattered, i.e., molecules that were indirectly affected by the presence of the capsule. Interesting aerodynamic features on blunt nose were observed from the results. It was found that the shock-wave standoff distance decreased with decreasing the altitude.

1. INTRODUCTION

One of the major programs of the Brazilian Program for Space Activities, officially called PNAE (acronyms for Programa Nacional de Atividades Espaciais) is related to a reusable orbital platform, named SARA, for scientific and technological experiments in low gravity environment. The system, build in a platform with a capsule shape, will stay in orbit during the time needed for the execution of the experiments, being sent back to the Earth, and then recovered.

In the development of a capsule platform, the aerothermodynamic aspects during the ballistic reentry flight offer exciting challenges to the aerodynamicists. The reentering trajectory of a capsule should be continuously under control to guarantee that it will not escape from the atmosphere, and that it will not exceed the heating and landing point limits. In the Earth atmosphere reentry, the capsule undergoes not only different velocity regimes – hypersonic, supersonic and subsonic – but also different flow regimes – free molecular flow, transition flow and continuum flow – and flight conditions that may difficult their aerodynamic design. In this context, a combination of engineering tools, experimental analysis, and numerical methods has been used in the design of high altitude reentry capsule aerodynamics. Nevertheless, due to difficulties and high costs associated to the experimental setup for high speed flows, a numerical analysis becomes imperative.

According to the current literature, many numerical studies and a few experimental investigations (Carlson, 1999; Gilmore and Crowther, 1995; Gnoffo, 1999; Gupta et al., 1996; Ivanov et al., 1998; Longo, 2003; Moss et al., 2006; Savino et al., 2005; Vashchenkov and Ivanov, 2002; Weiland et al., 2004; Wilmoth et al., 1997; Wood et al., 1996) have been dedicated to the aerothermodynamics of vehicles reentering the Earth atmosphere. Nevertheless, for the particular case of SARA capsule, only a few studies are available in the current literature (Pimentel et al., 2005; Sharipov, 2003; Tchuen et al., 2005; Toro et al., 2001; Sampaio and Santos, 2009, 2010). Given the number of papers on this subject, this introduction will focus on the more limited subject of SARA capsule .

Sharipov (2003) investigated the flowfield structure over the SARA capsule by employing the DSMC method. Argon was assumed as a working fluid with Mach numbers of 5, 10, and 20. Even considering that the real gas effect in a reentry capsule can not be simulated by a monatomic gas, that investigation might be considered as the first contribution to the aerothermodynamic analysis of the SARA capsule at high altitudes.

Pimentel et al. (2005) performed inviscid hypersonic flow simulations over the SARA capsule modeled by the planar two-dimensional and by the axisymmetric Euler equations. Results were presented for an altitude of 80 km, Mach numbers of 15 and 18, and angle of attack of 0 and 10 degrees. They also considered air as working fluid composed of five species (N_2, O_2, O, N, and NO) and their reactions of dissociation and recombination. Pressure and temperature contours were presented for 2-D and axisymmetric flows.

By using axisymmetric Navier-Stokes equations, Tchuen et al. (2005) have investigated the flowfield structure over the SARA capsule by considering hypersonic flow at zero angle of attack in chemical and thermal non-equilibrium. It was assumed air as working fluid composed of seven species (N_2, O_2, O, N, NO, NO^+, and e^-) and their reactions of dissociation and recombination. Results for pressure, skin friction, and heat transfer coefficients were presented for different combinations of Mach numbers of 10, 20 and 25 with altitudes of 75 and 80 km.

By means of the DSMC method, Sampaio and Santos (2009) have investigated the flowfield structure of a hypersonic flow over the SARA capsule in the reentry trajectory from 100 km to 85 km. This range basically covered the transition flow regime, $i.e.$, between the free collision flow and the continuum flow regime. The primary goal was to assess the sensitivity of the primary properties, velocity, density, pressure, and temperature, due to changes on the altitude

representative of a typically reentry trajectory of the SARA capsule.

Finally, Sampaio and Santos (2010) have extended the previous analysis (Sampaio and Santos, 2009) by examining computationally the aerodynamic surface quantities on the SARA capsule for the same reentry conditions. In this fashion, the purpose of the work was to assess the sensitivity of the heat transfer, pressure, skin friction and drag coefficients in the reentry trajectory from 100 km to 85 km.

In an effort to obtain further insight into the nature of the flowfield structure of the SARA capsule under hypersonic transition flow conditions, the present account extends the previously analysis (Sampaio and Santos, 2009, 2010) by examining computationally the shock-wave structure over the SARA capsule. In the present study effort is directed to assess the behavior of the shock-wave standoff distance, shock-wave thickness, and shock-wave shape along the reentry trajectory from 100 to 80 km of altitude.

The current proposed study focuses on the low-density region in the upper atmosphere, where the non-equilibrium conditions are such that traditional CFD calculations are inappropriate to yield accurate results. In such a circumstance, the Direct Simulation Monte Carlo (DSMC) method will be employed to calculate the rarefied hypersonic axisymmetric flow on the SARA capsule.

2. GEOMETRY DEFINITION

The SARA reentry capsule is an axisymmetric design consisting of a spherical nose with a 11.4-degree half-angle conical afterbody. The nose radius R is 0.2678 m, the afterbody base has a radius R_B of 0.5035 m, and the total length L is 1,410 m. Figure 1 illustrates schematically the capsule shape and the main important physical and geometrical parameters related to the hypersonic flow on the capsule. The main physical parameters are defined as follows: M_∞ is the freestream Mach number, Kn_∞ stands for the Knudsen number, α is the angle of attack, T_w is the wall temperature, and finally, α_n and σ_t represent the parameters related to the gas-surface interaction. In this fashion, the flowfield structure around the capsule may be affected by the effects of compressibility, rarefaction, gas-surface interaction, etc.

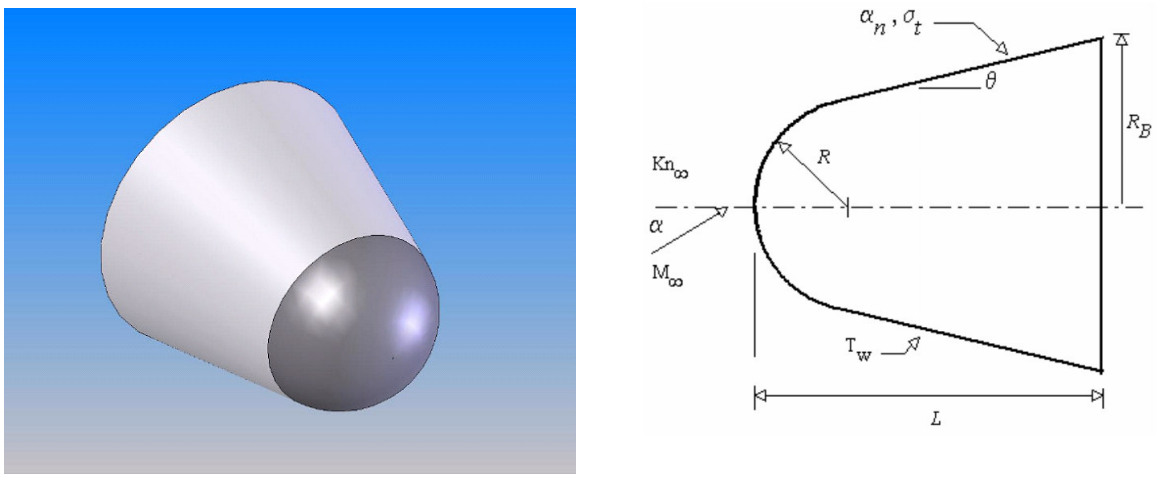

(a) (b)

Figure 1: Drawing illustrating (a) a schematic view of the capsule and (b) the important parameters.

3. COMPUTATIONAL TOOL

The Direct Simulation Monte Carlo (DSMC) method, pioneered by Bird (1994), has proved to be the most efficient technique for computing flowfields in which rarefaction effects play a significant role.

In the DSMC method, the gas is modeled at the microscopic level by using simulated particles, which each one represents a very large number of physical molecules or atoms. These representative molecules are tracked as they move, collide and undergo boundary interactions in simulated physical space. The molecular motion, which is considered to be deterministic, and the intermolecular collisions, which are considered to be stochastic, are uncoupled over the small time step used to advance the simulation and computed sequentially. The simulation is always calculated as unsteady flow. However, a steady flow solution is obtained as the large time state of the simulation.

In the DSMC algorithm, the linear dimensions of the cells should be small in comparison with the length scale of the macroscopic flow gradients normal to streamwise directions, which means that the cell dimensions should be the order of or smaller than the local mean free path (Alexander et al., 1998, 2000). The time step should be chosen to be sufficiently small in comparison with the local mean collision time (Garcia and Wagner, 2000; Hadjiconstantinou, 2000). In general, the total simulation time, discretized into time steps, is based on the physical time of the real flow. Finally, the number of simulated particles has to be large enough to make statistical correlations between particles insignificant.

The molecular collisions are modeled using the variable hard sphere (VHS) molecular model (Bird, 1981) and the no time counter (NTC) collision sampling technique (Bird, 1989). The VHS model assumes that the cross section of a molecule changes with the collision energy according to some power law. The exponent is calculated by matching the viscosity of the simulated gas to that of its real counterpart. In addition, the VHS model assumes an isotropic scattering in the center of mass frame of reference.

Simulations are performed using a non-reacting gas model consisting of two chemical species, N_2 and O_2. For polyatomic particles, transfer of energy to and from the internal modes has to be considered. In this way, energy exchanges between the translational and internal modes are considered. The energy exchange between kinetic and internal modes is controlled by the Borgnakke-Larsen statistical model (Borgnakke and Larsen, 1975). For a given collision, the probabilities are designated by the inverse of the relaxation numbers, which correspond to the number of collisions necessary, on average, for a molecule to relax. In this study, the relaxation numbers of 5 and 50 were used for the rotation and vibration, respectively.

4. COMPUTATIONAL FLOW DOMAIN AND GRID

For the numerical treatment of the problem, the flowfield around the capsule is divided into an arbitrary number of regions, which are subdivided into computational cells. The cells are further subdivided into subcells, two subcells/cell in each coordinate direction. The cell provides a convenient reference for the sampling of the macroscopic gas properties, while the collision partners are selected from the same subcell for the establishment of the collision rate. As a result, the physical space network is used to facilitate the choice of molecules for collisions and for the sampling of the macroscopic flow properties, such as velocity, density, pressure, temperature, etc.

The computational domain used for the calculation is made large enough so that body disturbances do not reach the upstream and side boundaries, where freestream conditions are specified. In this fashion, the computational domain changed according to the rarefaction de-

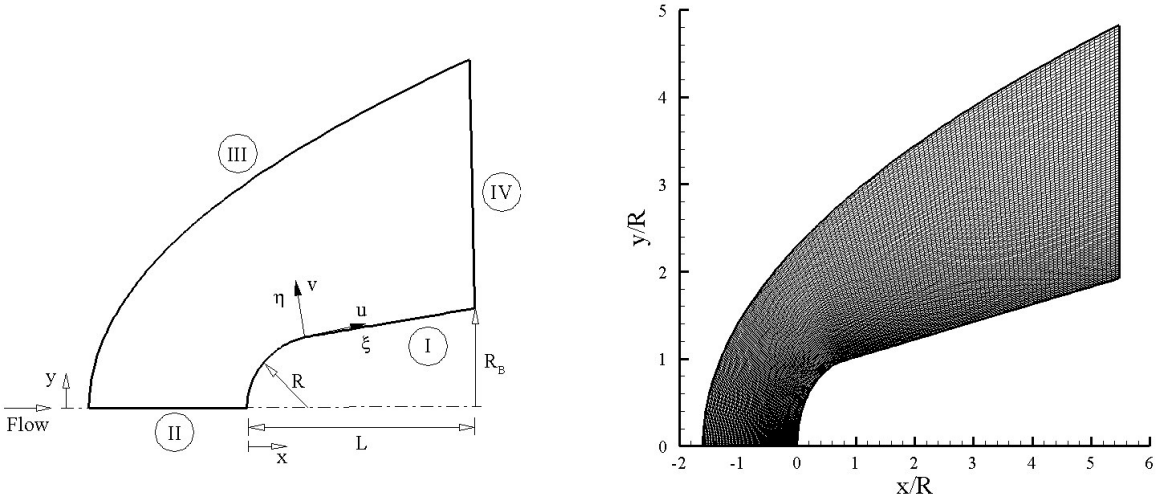

Figure 2: Drawing illustrating (a) the computational domain and (b) the standard grid for the 90 km case.

gree of the flow hitting the capsule. A schematic view of the computational domain is depicted in Fig. 2(a). According to this figure, Side I is defined by the capsule surface. Diffuse reflection with complete thermal accommodation is the condition applied to this side. In a diffuse reflection, the molecules are reflected equally in all directions, and the final velocity of the molecules is randomly assigned according to a half-range Maxwellian distribution determined by the wall temperature. Advantage of the flow symmetry is taken into account, and molecular simulation is applied to one-half of a full configuration. Thus, side II is a plane of symmetry, where all flow gradients normal to the plane are zero. At the molecular level, this plane is equivalent to a specular reflecting boundary. Side III is the freestream side through which simulated molecules enter and exit. Finally, the flow at the downstream outflow boundary, side IV, is predominantly supersonic and vacuum condition is specified (Bird, 1994). Therefore, at this boundary, simulated molecules can only exit.

The numerical accuracy in DSMC method depends on the cell size chosen, on the time step as well as on the number of particles per computational cell. These effects were investigated in order to determine the number of cells and the number of particles required to achieve grid independent solutions. The grid generation scheme used in this study follows that procedure presented by Bird (1994). Along the body surface (side I) and the outer boundary (side III), point distributions are generated in such way that the number of points on each side is the same; ξ-direction in Fig. 2(a). Then, the cell structure is defined by joining the corresponding points on each side by straight lines and then dividing each of these lines into segments which are joined to form the system of quadrilateral cells; η-direction in Fig. 2(a). The distribution can be controlled by a number of different distribution functions that allow the concentration of points in regions where high flow gradients or small mean free paths are expected.

A grid independence study was made with three different structured meshes in each coordinate direction. The effect of altering the cell size in the ξ-direction was investigated with grids of 60 (coarse), 120 (standard) and 180 (fine) cells, and 110 cells in the η-direction for the 90 km case. In analogous fashion, an examination was made in the η-direction with grids of 55 (coarse), 110 (standard) and 165 (fine) cells, and 120 cells in the ξ-direction for the same case.

From the total number of cells in the ξ-direction, 50 cells are located along the spherical nose and 70 cells distributed along the afterbody surface. In addition, each grid was made up of non-uniform cell spacing in both directions. The effect (not shown) of changing the cell size in both directions on the heat transfer, pressure and the skin friction coefficients was rather insensitive to the range of cell spacing considered, indicating that the standard grid, 120 X 110 cells, for the 90 km case, is essentially a grid independent. Figure 2(b) illustrates the standard grid for the 90 km case.

In a second stage of the grid independence investigation, a similar examination was made for the number of molecules. The standard grid for the 90 km case, 120 X 110 cells, corresponds to, on average, a total of 277,000 molecules. Two new cases using the same grid were investigated. These two new cases correspond to 131,600 and 396,100 molecules in the entire computational domain. As the three cases presented approximately the same results (not shown) for the heat transfer, pressure and skin friction coefficients, hence the standard grid with a total of 277,000 molecules is considered enough for the computation of the shock-wave structure.

As part of the validation process, the DSMC code was applied to a flat-ended circular cylinder in a rarefied hypersonic flow. Results for velocity, density, translational temperature, and rotational temperature distributions along the stagnation streamline were compared with those obtained from other established DSMC code in order to ascertain how well the DSMC code employed in this study is able to predict hypersonic rarefied flows. Since these data have been published elsewhere (Santos, 2009), the comparison will not be presented in this work.

5. FREESTREAM AND FLOW CONDITIONS

Flow conditions represent those experienced by the SARA capsule in the reentry from 100 to 80 km of altitude. Freestream flow conditions used for the numerical simulation of flow past the capsule are those given by Sampaio and Santos (2010) and summarized in Table 1, and the gas properties (Bird, 1994) are shown in Table 2. Referring to Table 1, T_∞, p_∞, ρ_∞, n_∞, λ_∞, and V_∞ stand respectively for temperature, pressure, density, number density, molecular mean free path, and velocity. According to Table 2, X, m, d and ω account respectively for mass fraction, molecular mass, molecular diameter and viscosity index.

Altitude (km)	T_∞(K)	p_∞(N/m^2)	ρ_∞(kg/m^3)	n_∞(m^{-3})	λ_∞(m)	V_∞(m/s)
80	180.7	1.03659	1.999×10^{-5}	4.1562×10^{20}	3.085×10^{-3}	7820
85	180.7	0.41249	7.956×10^{-6}	1.6539×10^{20}	7.751×10^{-3}	7864
90	180.7	0.16438	3.171×10^{-6}	6.5908×10^{19}	1.945×10^{-2}	7864
95	195.5	0.06801	1.212×10^{-6}	2.5197×10^{19}	5.088×10^{-2}	7866
100	210.0	0.03007	4.989×10^{-7}	1.0372×10^{19}	1.236×10^{-1}	7862

Table 1: Freestream flow conditions

	X	m (kg)	d (m)	ω
O_2	0.237	5.312×10^{-26}	4.01×10^{-10}	0.77
N_2	0.763	4.650×10^{-26}	4.11×10^{-10}	0.74

Table 2: Gas properties

According to the velocity-altitude map for the SARA capsule (Pessoa Filho, 2008), for altitudes of 80, 85, 90, 95 and 100 km, the freestream velocity V_∞ is 7820, 7864, 7864, 7866, and 7862 m/s, respectively. These values correspond to a freestream Mach number M_∞ of 29.0, 29.2, 29.2, 28.1, and 27.1, respectively. In the present account, the capsule surface was kept at a constant wall temperature T_w of 800 K for all cases investigated. This temperature is chosen to be representative of the surface temperature near the stagnation point of a reentry capsule.

The overall Knudsen number Kn is defined as the ratio of the molecular mean free path λ in the freestream gas to a characteristic dimension of the flowfield. In the present study, the characteristic dimension was defined as being the nose radius R. For the altitudes investigated, 80, 85, 90, 95, and 100 km, the overall Knudsen numbers correspond to Kn_R of 0.0115, 0.0289, 0.0726, 0.1899 and 0.4615, respectively. The Reynolds number Re_R correspond to 15249.5, 3442.7, 609.1, 224.1, and 92.2 for altitudes of 80, 85, 90, 95, and 100 km, respectively, based on conditions in the undisturbed stream with the nose radius R as the characteristic length. Finally, zero-degree angle of attack was considered in this investigation.

6. COMPUTATIONAL PROCEDURE

The problem of predicting the shape, thickness, and location of detached shock waves has been stimulated by the necessity for blunt noses and leading edges configurations designed for hypersonic flight in order to cope with the aerodynamic heating. In addition, the ability to predict the shape, thickness, and location of shock waves is of primary importance in analysis of aerodynamic interference.

In the present account, the shock-wave structure, defined by shape, thickness, and detachment of the shock wave, is predicted by employing a procedure based on the physics of the particles (Santos, 2008). In this respect, the flow is assumed to consist of three distinct classes of molecules; those molecules from the freestream that have not been affected by the presence of the leading edge are denoted as class I molecules; those molecules that, at some time in their past history, have struck and been reflected from the body surface are denoted as class II molecules; and finally, those molecules that have been indirectly affected by the presence of the body are defined as class III molecules. Figure 3 illustrates the definition for the molecular classes.

It is assumed that the class I molecule changes to class III molecule when it collides with class II or class III molecule. Class I or class III molecule is progressively transformed into class II molecule when it interacts with the body surface. Also, a class II molecule remains class II regardless of subsequent collisions and interactions. Therefore, the transition from class I molecules to class III molecules may represent the shock wave, and the transition from class III to class II may define the boundary layer.

A typical distribution of class III molecules along the stagnation streamline for blunt nose is demonstrated in Fig. 3 along with the definition used to determine the thickness, displacement and shape of the shock wave. In this figure, X is the distance x along the stagnation streamline normalized by the nose radius R, and f_{III} is the ratio of the number of molecules for class III to the total amount of molecules inside each cell.

In a rarefied flow, the shock wave has a finite region that depends on the transport properties of the gas, and can no longer be considered as a discontinuity obeying the classical Rankine-Hugoniot relations. In this scenario, the shock standoff distance Δ is defined as being the distance between the shock-wave center and the nose of the capsule along the stagnation streamline. As shown in Fig. 3, the shock-wave center is defined by the station that corresponds to the maximum value for f_{III}. The shock-wave thickness δ is defined by the distance between the stations that correspond to the mean value for f_{III}. Finally, the shock wave "location" is

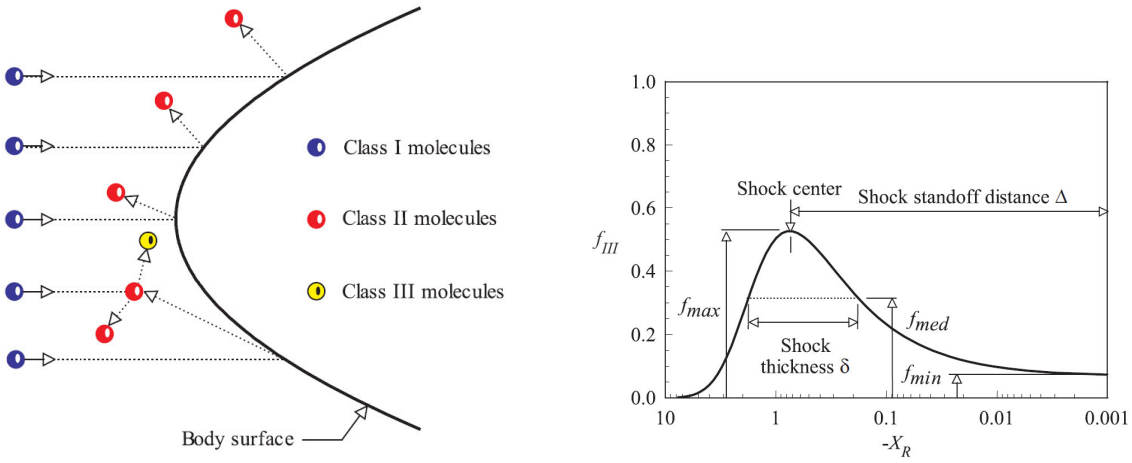

(a) (b)

Figure 3: Drawing illustrating the (a) classification of molecules, and the (b) definition of shock-wave structure.

determined by the coordinate points given by the maximum value in the f_{III} distribution along the lines departing from the body surface, i.e., η-direction as shown in Fig. 2(a).

7. COMPUTATIONAL RESULTS AND DISCUSSION

The purpose of this section is to discuss and to compare differences in the thickness, displacement, and shape of the shock wave during the reentry trajectory of the SARA capsule.

7.1 Molecular class distribution

The distribution of molecules for the three classes along the stagnation streamline is illustrated in Fig. 4 for altitudes of 100, 90 and 80 km. In this set of plots, f_I, f_{II} and f_{III} are the ratio of the number of molecules for class I, II and III, respectively, to the total amount of molecules inside each cell along the stagnation streamline, X_R is the distance x along the stagnation streamline normalized by the capsule nose radius R. Finally, the flow direction is from left to right, as defined in Fig. 2(a). In addition, plots on the left column present results in a linear scale in the abscissa, while those in the right column in a logarithm scale. Furthermore, results for altitudes of 95 and 85 km are intermediate, and they will not be shown.

Interesting flow features may be recognized in these plots. The freestream molecules are identified by class I molecules. In this way, the upstream effects due to presence of the capsule may be inferred from the distribution for class I molecules. By considering the upstream disturbance domain given by the section X_R that corresponds to the f_I ratio of 0.99, then it is found a X_R of -1.96, -0.79, and -0.29 for 100, 90, and 80 km of altitude. This is an expected behavior in the sense that, as the altitude decreases the number density increases and the molecules reflecting from the nose region do not get to travel far from the nose in the upstream direction.

Another feature of great significance in these plots is the behavior for the class I molecules. It should be noticed that molecules from freestream, represented by class I molecules, collide with the capsule nose, at least a small amount, for the 100 km case, after the establishment of the steady state. In contrast, molecules from freestream basically do not reach the nose of the capsule for the case 80 km case. This is explained by the fact that density (Sampaio and Santos,

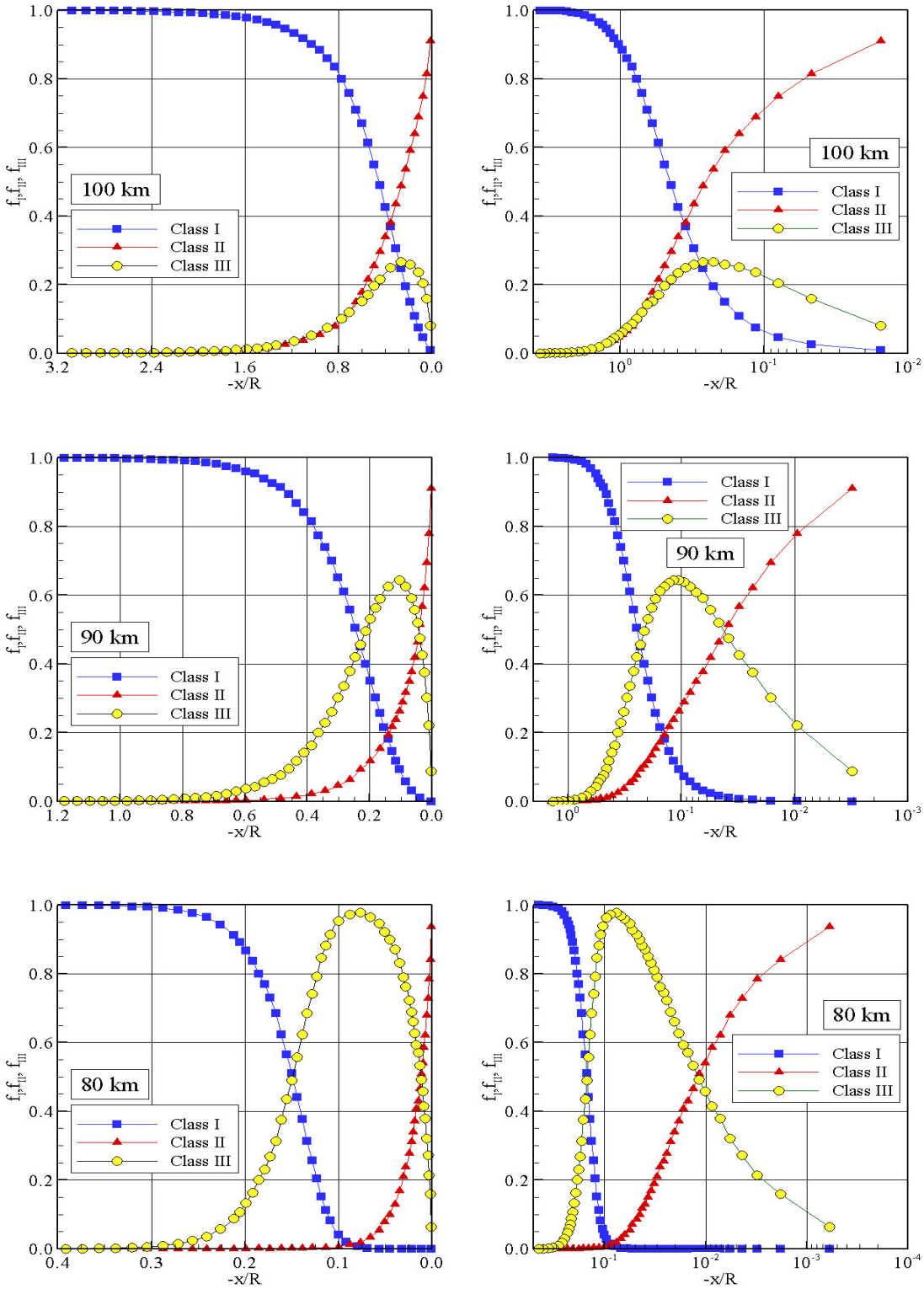

Figure 4: Distributions of molecules for classes I, II and III along the stagnation streamline for 100, 90 and 80 km of altitude.

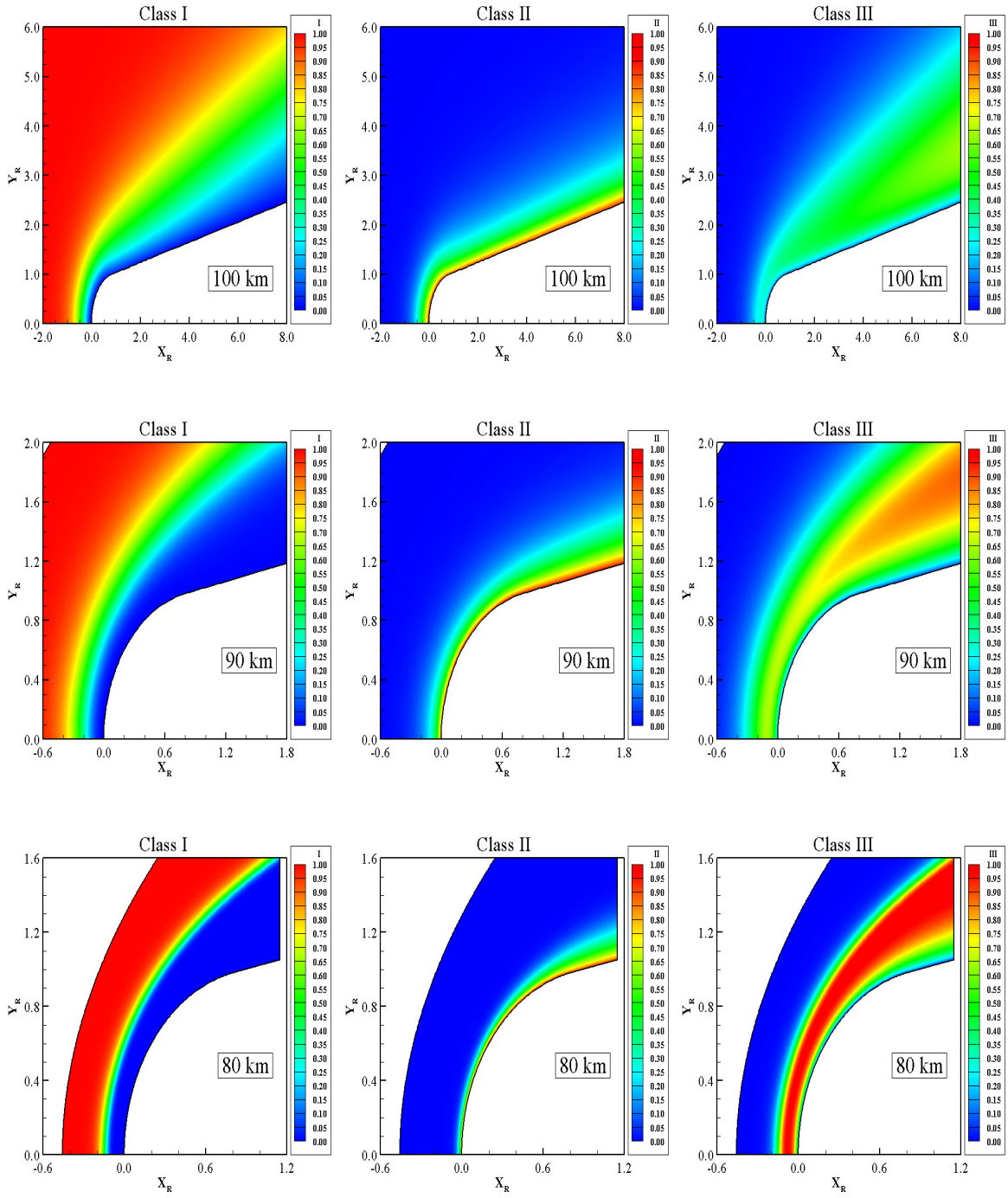

Figure 5: Distributions of molecules for classes I, II and III in the entire computational domain for 100, 90 and 80 km of altitude.

2009) increases with decreasing the altitude in the stagnation region and reaches its maximum value at the stagnation point. In this connection, the buildup of particle density near the nose capsule acts as a shield for the molecules coming from the undisturbed stream. As a base of comparison, the density ratio ρ/ρ_∞ is around 35.4, 59.9, and 91.6 for 100, 90, and 80 km of altitude.

Another flow peculiarity is related to the distribution of class II molecules. As mentioned earlier, class II molecules may represent the boundary layer. It is clearly noticed that the boundary-layer thickness decreases with decreasing the altitude. The boundary-layer thickness varies inversely with the Reynolds number. For high altitudes, the boundary-layer thickness on hypersonic vehicles can be large relative to the shock-layer thickness. As the SARA capsule enters into the earth atmosphere, from 100 km to 80 km, the Reynolds number increases, as showed in previous sections. As a result, the boundary-layer thickness decreases.

Having a clear qualitative picture of the molecular class distribution along the stagnation streamline, it proves instructive to illustrate the differences in the molecular class distribution in the entire computational domain. In doing so, Figure 5 illustrates contour maps for class I, II and III, related to the capsule at 100, 90, and 80 km of altitude.

7.2 Shock-wave standoff distance

According to the definition shown in Fig. 3(b), the shock-wave standoff distance Δ can be estimated in Fig. 4 for the altitudes shown. It is apparent from these plots that there is a discrete shock-wave standoff distance for the cases investigated.

The calculated shock-wave standoff distance Δ, normalized by the capsule nose radius R, and by the freestream mean free path λ_∞, is tabulated in Table 3 for the cases investigated. It is important to recall that the freestream mean free path λ_∞ depends on the altitude. As would be expected, the shock standoff distance decreases with decreasing the altitude, i.e., with decreasing the Knudsen number Kn_R. As a reference, the shock-wave standoff distance for the 100 km case is around 3.0 times larger than that for the 80 km case. For convenience, Fig. 6(a) illustrates the shock-wave standoff distance, Δ/R as a function of the altitude.

	100 km	95 km	90 km	85 km	80 km
Δ/R	0.244	0.160	0.111	0.090	0.080
Δ/λ_∞	0.528	0.842	1.524	3.109	6.960

Table 3: Shock-wave standoff distance Δ for the SARA capsule.

7.3 Shock-wave thickness

Based on the definition of the shock-wave thickness shown in Fig. 3(b), the shock-wave thickness δ along the stagnation streamline can be obtained in Fig. 4 for the cases shown. As a result of the calculation, Table 4 tabulates the shock-wave thickness δ, normalized by the nose radius R and by the freestream mean free path λ_∞.

	100 km	95 km	90 km	85 km	80 km
δ/R	0.488	0.359	0.247	0.178	0.135
δ/λ_∞	1.057	1.889	3.405	6.161	11.694

Table 4: Shock-wave thickness δ for the SARA capsule.

As a result of the simulation, the shock-wave thickness for the 100 km case is around 3.6

times larger than that for the 80 km case. As a base of comparison, Fig. 6(a) displays the shock-wave thickness, δ/R as a function of the altitude.

7.4 Shock-wave shape

The shock-wave shape, defined by the shock-wave center location, is obtained by calculating the position that corresponds to the maximum f for class III molecules in the η-direction (see Fig. 2) along the body surface. In doing so, the shock-wave shape on the SARA capsule is demonstrates in Fig. 6(b) for the altitude range investigated. In this figure, X_R and Y_R are the Cartesian coordinates x and y normalized by the nose radius R. According to this figure, it is firmly established that the shock-wave shape is affected by the altitude, i.e., by the Knudsen number Kn_R, as expected. It is seen that the shock-layer around the stagnation region increases with increasing the altitude. The reason for that is because with the altitude rise, the molecules reflect from the body surface penetrate further in the off-body direction.

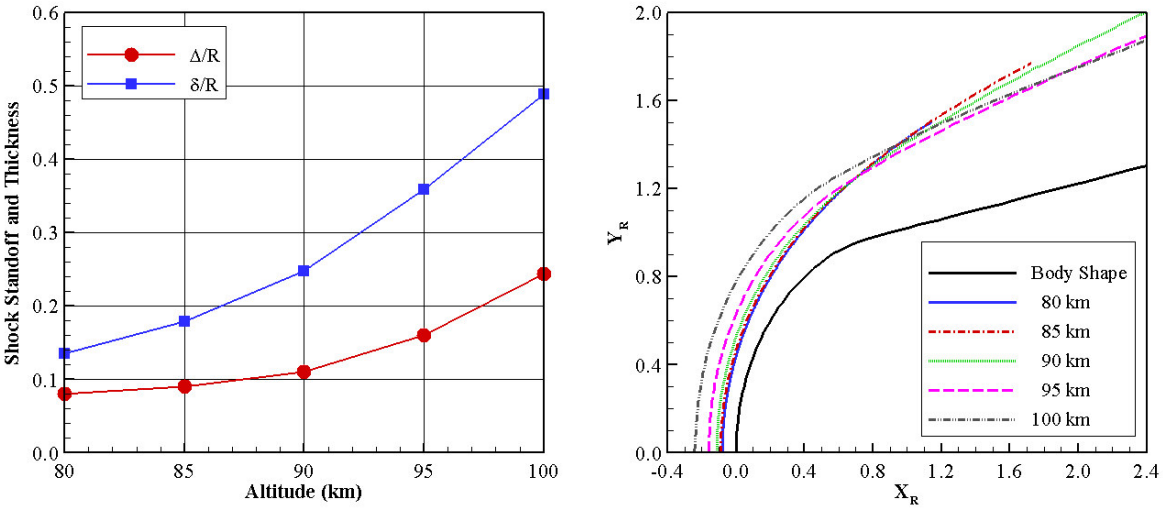

(a) (b)

Figure 6: (a) Shock-wave standoff distance and shock-wave thickness, and (b) shock-wave shape.

8. CONCLUDING REMARKS

This study applies the Direct Simulation Monte Carlo method to investigate the shock-wave structure on a Brazilian reentry capsule. Calculations have provided information concerning the nature of the shock-wave detachment distance, shock-wave thickness, and shock-wave shape along the capsule reentry trajectory from 100 to 80 km of altitude for the idealized situation of axisymmetric hypersonic rarefied flow. The analysis showed that the shock-wave structure was affected by changes on the altitude. It was found that the shock-wave standoff and the shock-wave thickness decreased by decreasing the altitude for the conditions investigated. In addition, the shock-wave center was displaced close to the capsule nose with decreasing the altitude.

9. ACKNOWLEDGEMENTS

The authors would like to thank the financial support provided by FAPESP (Fundação de Amparo a Pesquisa do Estado de São Paulo) under Grant No. 2008/03878-9.

REFERENCES

Alexander, F. J., Garcia, A. L., and Alder, B. J., Cell size dependence of transport coefficient in stochastic particle algorithms. *Physics of Fluids*, 10:1540–1542, 1998.

Alexander, F. J., Garcia, A. L., and Alder, B. J., Erratum: Cell size Dependence of transport coefficient in stochastic particle algorithms. *Physics of Fluids*, 12:731–731, 2000.

Bird, G. A., Monte Carlo simulation in an engineering context. *Progress in Astronautics and Aeronautics: Rarefied gas Dynamics*, ed., Fisher, S. S., AIAA New York, 74:239–255, 1981.

Bird, G. A., Perception of numerical method in rarefied gasdynamics. *Rarefied Gas Dynamics: Theoretical and Computational Techniques*, Progress in Astronautics and Aeronautics, eds. Muntz, E. P., Weaver, D. P.and Capbell, D. H., AIAA, New York, 118:374–395, 1989.

Bird, G. A., *Molecular gas dynamics and the direct simulation of gas flows*. Oxford University Press, 1994.

Borgnakke, C. and Larsen, P. S., Statistical collision model for Monte Carlo simulation of polyatomic gas mixture. *Journal of Computational Physics*, 18:405–420, 1975.

Carlson, H. A., Aerothermodynamic analyses of hypersonic, blunt-body flows. *Journal of Spacecraft and Rockets*, 36:912–915, 1999.

Garcia, A. L., and Wagner, W., Time step truncation error in direct simulation Monte Carlo. *Physics of Fluids*, 12:2621–2633, 2000.

Gilmore, M. R., and Crowther, R., Direct simulation and test particle Monte-Carlo, and Navier-Stokes predictions of the re-entry state of the FSW-1 satellite. *Proceedings of the 19th International Symposium on Rarefied Gas Dynamics*, eds. Harvey, J. and Lord, G., Oxford, University Press, 2:1387–1393, 1995.

Gnoffo, P., Planetary-entry gas dynamics. *Annual Review of Fluid Mechanics*, 31:459–494, 1999.

Gupta, R. N., Moss, J. N., and Price, J. M., Assessment of thermochemical nonequilibrium and slip effects for orbital reentry experiment (OREX). *Proceedings of the 31st AIAA Thermophysics Conference*, AIAA Paper 1996–1859, New Orleans, LA, Jun 17–20, 1996.

Hadjiconstantinou, N. G., Analysis of discretization in the direct simulation Monte Carlo. *Physics of Fluids*, 12:2634–2638, 2000.

Ivanov, M. S., Markelov, G. N., Gimelshein, S. F., Mishina, L. V., Krylov, A. N., and Grechko, N. V., High-altitude capsule aerodynamcis with real gas effects. *Journal of Spacecraft and Rockets*, 35:16–22, 1998.

Longo, J. M. A., Aerothermodynamics – A critical review at DLR. *Aerospace Science and Techonology*, 7:429–438, 2003.

Moss, J. N., Glass, C. E., and Greene, F. A., Blunt body aerodynamics for hypersonic low density flows. *Proceedings of the 25th International Symposium on Rarefied Gas Dynamics*, Saint Petersburg, Russia, 2006.

Pessoa Filho, J. B., Velocity-altitude map for SARA capsule. *Private Communication*, 2008.

Pimentel, C. A. R., Azevedo, J. L. F., Korzenowski, H., and Mantelli, M. B. H., Chemical equilibrium inviscid flow over SARA re-entry vehicle. *Proceedings of the 43rd AIAA Aerospace Sciences Meeting and Exhibit*, AIAA Paper 2005–0390, Reno, NV, Jan 10–13, 2005.

Sampaio, P. A. C., and Santos, W. F. N., Aerothermodynamic analysis of a reentry Brazilian satellite. *Proceedings of the 30th Iberian-Latin-American Congress on Computational Methods in Engineering*, Armação de Búzios, RJ, Brazil, 2009.

Sampaio, P. A. C., and Santos, W. F. N., Computational analysis of the aerodynamic heating and drag of a reentry Brazilian satellite. *Proceedings of the 6th National Congress of Mechanical Engineering*, Campina Grande, PB, Brazil, 2010.

Santos, W. F. N., Some physical and computational aspects of shock wave over power-law leading edges. *Physics of Fluids*, 20:016101–11, 2008

Santos, W. F. N., DSMC calculations of rarefied hypersonic flow over a flat-ended cylinder. In XII Encontro de Modelagem Computacional, Rio de Janeiro, RJ, Brazil, Dec 2-4, 2009.

Savino, R., Fumo, M. S., Paterna, D., and Serpico, M., Aerothermodynamic study of UHTC-based thermal protection systems. *Aerospace Science and Techonology*, 9:151–160, 2005.

Sharipov, F., Hypersonic flow of rarefied gas near the Brazilian satellite during its reentry into atmosphere. *Brazilian Journal of Physics*, 33:398–405, 2003.

Tchuen, G., Burtschell, Y., and Zeitoun, D. E., Numerical prediction of nonequilibrium hypersonic flow around Brazilian satellite SARA. *Brazilian Journal of Physics*, 35:148–156, 2005.

Toro, P. G. P., Minucci, M. A. S., Ramos, A. G., Chanes Jr., J. B., Pereira, A. L., Korzenowski, H., Nagamatsu, H. T., and Myrabo, L. N., Experimental investigation of blunt body at Mach 8. *Proceedings of the 39th AIAA Aerospace Sciences Meeting and Exhibit*, AIAA Paper 2001–0644, Reno, NV, Jan 8–11, 2001.

Vashchenkov, P. V., and Ivanov, M. S., Numerical analysis of high-altitude aerothermodynamics of expert reentry vehicle. *Proceedings of the International Conference on the Methods of Aerophysical Research*, Russia, 2002.

Weiland, C., Longo, J., Gülhan, A., and Decker, K., Aerothermodynamics for reusable lanch systems. *Aerospace Science and Techonology*, 8:101–110, 2004.

Wilmoth, R. G., Mitcheltree, R. A., and Moss, J. N., Low-density aerodynamics of the stardust sample return capsule. *Proceedings of the 32nd AIAA Thermophysics Conference*, AIAA Paper 1997–2510, Atlanta, Ga, Jun 23–25, 1997.

Wood, W. A., Gnoffo, P. A., and Rault, D. F. G., Aerodynamic analysis of commercial experiment transporter re-entry capsule. *Journal of Spacecraft and Rockets*, 33:643–646, 1996.